Carbohydrate Polymers 87 (2012) 53–60

Contents lists available at ScienceDirect

Carbohydrate Polymers

journal homepage: www.elsevier.com/locate/carbpol

Clay nanopaper composites of nacre-like structure based on montmorrilonite and cellulose nanofibers—Improvements due to chitosan addition

Andong Liu[a,b], Lars A. Berglund[a,b,*]

[a] Department of Fibre and Polymer Technology, Royal Institute of Technology, SE-10044 Stockholm, Sweden
[b] Wallenberg Wood Science Center and Department of Fiber and Polymer Technology, Royal Institute of Technology, SE-10044 Stockholm, Sweden

ARTICLE INFO

Article history:
Received 24 May 2011
Received in revised form 27 June 2011
Accepted 7 July 2011
Available online 19 July 2011

Keywords:
Nanofibrillated
Nanocomposite
Flocculation
Gas barrier
Packaging

ABSTRACT

Clay nanopaper are nanocomposites with nacre-like structure and multifunctional characteristics including high modulus, significant strength and toughness as well as fire retardancy and low oxygen transmission rate (OTR). Montmorrilonite (MTM) and nanofibrillated cellulose (NFC) hydrocolloids are combined with a chitosan (CS) solution to form high MTM content nanopaper structures by the use of a previously developed papermaking approach. Chitosan functions as flocculation agent and decreases dewatering time to less than 10% compared with MTM–NFC clay nanopaper. The effect of chitosan on the clay nanopaper structure was studied by X-ray diffraction (XRD), scanning electron microscopy (SEM) and Fourier transform infrared (FTIR) spectroscopy. Properties were measured by uniaxial tensile testing, thermogravimetric analysis (TGA), OTR and moisture adsorption experiments. A nacre-like multilayered structure was confirmed and the chitosan–clay nanopaper showed favorable mechanical properties at clay contents as high as 44–48 wt%.

1. Introduction

Clay nanocomposites with biobased polymer matrices are of increasing scientific and industrial interest. Favorable characteristics include improved Young's modulus, reduced gas permeability, improved fire retardancy. In addition, the origin of the polymer matrix from renewable resources is an advantage as well as the biodegradable character of the organic components. Potential applications include melt-processed thermoplastic mouldings, packaging films and coatings. Examples of materials include polylactide/clay nanocomposites (Maiti, Yamada, Okamoto, Ueda, & Okamoto, 2002; Ray, Maiti, Okamoto, Yamada, & Ueda, 2002), poly(butylene succinate)/clay nanocomposites (Ray, Okamoto, & Okamoto, 2003), furfuryl alcohol/clay nanocomposites (Pranger & Tannenbaum, 2008), soy protein resin/clay nanocomposites (Huang & Netravali, 2007), and cellulose acetate/clay nanocomposites (Park, Liang, Mohanty, Misra, & Drzal, 2004).

More advanced clay nanocomposites are prepared from layer-by-layer assembly (Podsiadlo et al., 2007; Tang, Kotov, Magonov, & Ozturk, 2003) and by combining Al_2O_3 with chitosan (Bonderer, Studart, & Gauckler, 2008). In these cases, the inorganic platelet reinforcement is ordered parallel to the film surface. Podsiadlo et al. (2007) used high inorganic content and the layered "brick-and-mortar" structure is inspired by nacre, which is a biological composite of high toughness. A limitation with the mentioned studies is that preparation procedures are quite cumbersome. The studies by Walther, Bjurhager, Malho, Pere, et al. (2010) and Walther, Bjurhager, Malho, Berglund, and Ikkala (2010) are therefore important. The polymer matrix is adsorbed to the clay platelets. The resulting hydrocolloid is simply filtrated in a papermaking type of process to form remarkably well-ordered nanocomposites of nacre-like structure and favorable mechanical properties. In a similar procedure published later, MTM clay is combined with chitosan (Yao, Tan, Fang, & Yu, 2010). MTM can also be combined with cellulose nanofibers in the form of nanofibrillated cellulose (NFC) from wood (Liu, Walther, Ikkala, Belova, & Berglund, 2011). The oxygen barrier properties in the dry state were very good. The oxygen transmission rate was below the detection limit of the instrument. In addition, the use of a cellulose nanofiber matrix provided new deformation mechanisms so that ductility and toughness were quite high, despite an inorganic content as high as 89 wt%. In the present study the NFC matrix in clay nanopaper is combined with a biopolymer.

Chitosan, poly-(1,4)-2-amino-2-deoxy-D-glucose, is the deacetylated product of chitin, poly(N-acetyl-D-glucoseamine), and is often denoted CS in the present study. Because of its biodegradability, biocompatibility, and antimicrobial activity, chitosan has been extensively studied for applications in food

* Corresponding author at: Wallenberg Wood Science Center and Department of Fiber and Polymer Technology, Royal Institute of Technology, SE-10044 Stockholm, Sweden. Tel.: +46 8 7908118; fax: +46 8 7908101.
E-mail address: blund@kth.se (L.A. Berglund).

0144-8617/$ – see front matter © 2011 Published by Elsevier Ltd.
doi:10.1016/j.carbpol.2011.07.019

packaging, biomedical implants, and water treatment etc. Chitosan is readily protonated in organic acids, due to the acidity of the $-NH_3^+$ group ($pK_a = 6.3$) (Papineau, Hoover, Knorr, & Farkas, 1991). Under acidic condition, chitosan is positively charged and can bind to negatively charged substances. For this reason, chitosan–clay nanocomposites are interesting (Darder, Colilla, & Ruiz-Hitzky, 2003; Günister, Pestreli, Ünlü, Atıcı, & Güngör, 2007). MTM has a layered structure with large adsorption capacity for polymer molecules. Non-ionic polymers can adsorb to the MTM surface by steric interactions, whereas ionic polymers induce electrostatic interaction. Further, MTM with negative charge on the surface exhibit an inhibitory property for proliferation of bacteria. So negatively charged MTM can be combined with chitosan via electrostatic interactions and flocculation is likely to occur (Divakaran & Pillai, 2001; Roussya, Voorenb, Dempseyc, & Guibal, 2005). The combination of MTM and CS results in excellent inhibition properties for bacterial growth (Wang et al., 2006). However, film strength is below 50 MPa and film-forming characteristics poor.

In a previous study NFC nanofibers reinforced chitosan matrices of different molecular weight and degree of substitution (Fernandes et al., 2010). The strength properties of the NFC–CS nanocomposites were improved from 50 MPa to 110 MPa. The MTM–NFC clay nanopaper already mentioned is also an inspiration for the present study, and here NFC forms a network matrix for dispersed MTM platelet aggregates (Liu et al., 2011). Clay nanopaper can have high inorganic content and has a multilayered structure. These nanostructural features result in good mechanical properties, heat endurance, flame retardance and oxygen barrier properties. For example, the oxygen transmission rate (OTR) of clay nanopaper with 50 wt% clay was less than 0.001 $cm^3\,mm\,m^{-2}\,day^{-1}\,atm^{-1}$ at dry condition. However, a serious limitation with the technology is that the papermaking process step is fairly slow. The main bottleneck is the dewatering phase during filtration. It is quite slow and this is an obvious obstacle for industrial mass production. Furthermore, there is only weak interaction between NFC and MTM, and OTR increases strongly at high relative humidity. Most likely, the reason is moisture adsorption and swelling of MTM–NFC clay nanopaper. Possibly, addition of chitosan may have beneficial effects.

In the present study, protonated chitosan is used to modify MTM–NFC clay nanopaper by dispersion blending utilizing ionic interaction. The effect of chitosan addition on preparation time for the clay nanopaper is of great interest. An important objective is also to study the effect of chitosan addition on structure and properties of clay nanopaper.

2. Experimental

2.1. Materials

The clay was a sodium montmorillonite (Cloisite Na^+, Southern Clay Products) with a cation-exchange capacity (CEC) of 92 mequiv./100 g. The average size of the platelets is 110 nm as described by the manufacturer. 1.0 wt% MTM dispersion, used in the experiments, was prepared by dispersing 10 g of MTM in 1 L of de-ionized water under vigorous stirring.

NFC was prepared by enzymatic pretreatment of wood pulp followed by mechanical homogenization (Henriksson, Henriksson, Berglund, & Lindström, 2007). The nanofibers are typically around 15 nm in diameter and several micrometers in length. The degree of polymerization (DP) of the cellulose in the nanofibers was estimated to 480 based on the average intrinsic viscosity after homogenization. A colloidal NFC dispersion with 1.63 wt% solid content was obtained, and stored at 4 °C.

Chitosan of high molecular weight (M_W average 342,500 g mol^{-1}) was used. It contains an average number of glucosamine units of 2130 (glucosamine M_W 161 g mol^{-1}), and was supplied by Aldrich. 0.5% (w/v) chitosan solutions were prepared by the addition of corresponding amounts of polysaccharide to 1% (v/v) acetic acid (Merck). After stirring of the resulting solution for about 2 h, the pH of the polysaccharide solution was adjusted to 4.9 with NaOH before mixing with the MTM or MTM–NFC colloidal dispersions.

2.2. Preparation of nanocomposites

2.2.1. Chitosan (CS) modified MTM–NFC clay nanopaper

First, an MTM–NFC dispersion (0.62 wt%/0.62 wt%) with a weight ratio of 1:1 was prepared. 613 g NFC dispersion (solid content 1.63 wt%) was added to 1000 g MTM dispersion (solid content 1.0 wt%), and stirred at least 4 h. The co-dispersion was subjected to vigorous stirring before use. Chitosan solutions with 0.2 g, 0.4 g, and 1.0 g of biopolymer were slowly added to 163 g MTM–NFC co-dispersion, at 80 °C, to obtain clay nanopaper with initial chitosan–MTM–NFC ratios of 10:50:50, 20:50:50, and 50:50:50, coded as CS10–MTM50–NFC50, CS20–MTM50–NFC50, CS50–MTM50–NFC50, respectively. The mixed dispersions were stirred for 2 h and washed with de-ionized water until free from acetate. Then the mixtures were vacuum-filtrated by Rapid Köthen using a filter membrane, 0.65 μm DVPP, Millipore, USA (Sehaqui, Liu, Zhou, & Berglund, 2010). The filtration time was only 2–3 min. After filtration, the wet films were carefully peeled off from the filtration membrane, stacked between metal grids and placed between two filter papers. Finally, clay nanopaper with a thickness in the range of 90–100 μm was obtained by vacuum drying at 93 °C for 10–15 min (Sehaqui et al., 2010).

2.2.2. CS–NFC nanopaper

Chitosan solutions containing 0.1 g, 0.2 g, 0.3 g of biopolymer were slowly added to 500 g NFC dispersion (solid content 0.2 wt%), at 80 °C, to obtain nanocomposites with initial chitosan–NFC ratios of 10:100,20:100, 30:100, coded as CS10–NFC100, CS20–NFC100, CS30–NFC100. The mixed dispersion was stirred for 2 h and washed with de-ionized water until free from acetate. Finally, CS–NFC nanopaper was obtained according to the method of CS–MTM–NFC.

2.2.3. CS–MTM nanocomposites

Chitosan solutions containing 0.2 g, 0.4 g, 1.0 g of biopolymer were slowly added to 100 g 1.0 wt% MTM dispersion, at 80 °C, to obtain nanocomposites with initial chitosan–MTM ratios of 20:100, 40:100, 100:100, coded as CS20–MTM100, CS40–MTM100, CS100–MTM100, respectively. The mixed dispersion was stirred for 2 h and washed with de-ionized water until free from acetate. Finally, CS–MTM nanocomposites were prepared according to the method used for CS–MTM–NFC.

2.2.4. NFC reinforced CS–MTM nanocomposites

Chitosan solutions containing 1.0 g of biopolymer were slowly added to 100 g 1.0 wt% MTM dispersion. The mixed dispersion was stirred for 2 h and washed with de-ionized water until free from acetate. Then CS/MTM was redispersed in water and stirred for 2 h. Then 4 wt%, 8 wt% and 12 wt% NFC in total weight were added to the CS/MTM dispersion and stirred for 24 h. Finally, CS–MTM films with different NFC contents were obtained according to the method used for CS–MTM–NFC. The samples were coded as CS50–MTM50–NFC4, CS50–MTM50–NFC8 and CS50–MTM50–NFC12.

Table 1 shows all information of the initial components of samples in aqueous solutions/dispersions.

Table 1
The notation used for different materials, and the corresponding composition expressed as parts by weight (pbw).

Samples	Chitosan (pbw)	MTM (pbw)	NFC (pbw)
CS20–MTM100	20	100	0
CS40–MTM100	40	100	0
CS100–MTM100	100	100	0
NFC	0	0	100
CS10–NFC100	10	0	100
CS20–NFC100	20	0	100
CS30–NFC100	30	0	100
MTM50–NFC50	0	50	50
CS10–MTM50–NFC50	10	50	50
CS20–MTM50–NFC50	20	50	50
CS50–MTM50–NFC50	50	50	50
CS50–MTM50–NFC4	50	50	4
CS50–MTM50–NFC8	50	50	8
CS50–MTM50–NFC12	50	50	12

2.3. Characterization of nanocomposites

2.3.1. X-ray diffraction (XRD)

XRD patterns of the films were recorded by a Siemens D5000 X-ray diffractometer at room temperature. The CuKR radiation source was operated at 40 kV and 40 mA. Patterns were recorded by monitoring diffractions from 1° to 10°. The scan speed was 2°/min.

2.3.2. Fourier transform infrared (FTIR) spectra

FTIR spectra (transmission) were measured on a Perkin-Elmer FTIR spectrophotometer 2000 in the range of 4000–400 cm^{-1} at a resolution of 4 cm^{-1}.

2.3.3. Scanning electron microscopy (SEM)

The morphology was examined with a JEOL JSM-820 Scanning Microscope. The samples were held in liquid N_2 and a brittle fracture was performed. A few nm thick layer of gold was sputtered onto the surface of cross-sections prior to imaging.

2.3.4. Tensile testing

The tensile tests of the films were performed with a Universal Materials Testing Machine from Instron, USA, equipped with a 100 N load cell. Specimens of 40 mm length and 60–80 μm thickness and 5 mm width were tested with strain rate of 4 mm/min. The relative humidity was kept at 50% and the temperature at 23 °C. The specimens were conditioned for at least 48 h in this environment prior to testing. The displacement was measured by Digital Speckle Photography (DSP). A pattern was prepared for the DSP by applying printer toner to the sample surface. During tensile test images of the whole specimen was taken. The frame rate was set to 5 fps. The results for each material are based on at least 6 specimens, if nothing else is mentioned.

2.3.5. Density measurements, porosity and volume fraction calculations

The density of the materials (ρ_{ce}), including porosity, is determined from samples ca. 2 cm wide and 4 cm long by measuring the weight of the sample in air (W_a) and immersed in mercury (W_{Hg}). Knowing the density of mercury (ρ_{Hg} = 13.534 g cm^{-3}), and that of air (ρ_{air} = 0.0013 g cm^{-3}), the density of the sample is given by:

$$\rho_{ce} = \frac{W_a}{W_a - W_{Hg}} \times (\rho_{Hg} - \rho_{air}) \quad (1)$$

Porosity defined as the volume fraction of voids (V_v) is calculated according to the following equations:

$$V_V = 1 - \left(\frac{\rho_{ce}}{\rho_{ct}}\right) \quad (2)$$

$$\rho_{ct} = \frac{1}{\sum_{i=1}^{n}(W_i/\rho_i)} \quad (3)$$

where ρ_{ct} is the density of the solid constituting the composite (i.e. the density of non-porous composite), which was calculated from the densities, ρ_i, of the constituents ($i = 1, 2, \ldots, n$) and their weight fractions, W_i.

The density of chitosan is assumed to be 1280 kg m^{-3}. The density of cellulose is assumed to be 1460 kg m^{-3}, while the density of MTM is assumed to be 2860 kg m^{-3}. The volume fractions (V_i, $i = 1, 2, \ldots, n$) of chitosan NFC and MTM are calculated from the weight fraction of NFC and from the density of the films according to the following equations:

$$V_i = (1 - V_V) \times \frac{\rho_{ct}}{\rho_i} \times W_i \quad (4)$$

2.3.6. Thermogravimetric analysis (TGA)

The TGA was conducted on a Perkin-Elmer TGA 7-thermal analyzer from 25 to 800 °C with a heating rate of 10 °C/min under oxygen with flow rate 50 ml/min.

2.3.7. Oxygen transmission rate (OTR)

The permeability of the material to oxygen at 23 °C was determined using a Mocon OX-TRAN TWIN equipped with a coulometric oxygen sensor. Degassed film samples with thickness of 95 ± 5 μm were mounted in an isolated diffusion cell and were subsequently surrounded by flowing nitrogen gas to remove sorbed oxygen from the samples. The sample had a circular exposure area of 100×10^{-4} m^2 achieved by covering a part of the film with a tight aluminum foil that has an adhesive on its surface. One side of the sample was initially exposed to flowing oxygen containing 1% hydrogen at atmospheric pressure. The oxygen pressure was zero on the other side. The flow rate (Q) through the sample was measured and, from the steady-state flow rate (Q_∞), the oxygen permeability coefficient (P) was calculated.

2.3.8. Dynamic vapor sorption (DVS)

The kinetics of water sorption of films was measured using a Dynamic Vapor Sorption apparatus from Surface Measurement System. The sample was dried at RH 0%, 30 °C until a constant weight was attained. Then the test began at RH 50%, 30 °C until a constant weight was attained.

3. Results and discussion

3.1. Interaction between chitosan, NFC and MTM

Fig. 1 shows photographs of the hydrocolloid co-dispersion of MTM–NFC (weight ratio = 50/50) before and after adding 10 parts by weight of positively charged chitosan (CS10–MTM50–NFC50). The MTM–NFC co-dispersion is very homogeneous and it is also stable. The main reason is that there are hydroxyl groups and some negative charge on the surface of NFC and MTM. Hydroxyl groups provide hydrophilicity and the charge makes the NFC and MTM nanoparticles easier to disperse since they repel each other. The mixed hydrocolloid is well dispersed. When a total of 10 parts by weight dry content of positively charged chitosan solution was added dropwise into the MTM50–NFC50 co-dispersion, the upper part of the dispersion becomes transparent after a short period, see Fig. 1(B). This indicates immediate flocculation due to electrostatic interaction, as discussed in previous studies (Divakaran & Pillai, 2001; Roussya et al., 2005). Positively charged chitosan acts as a flocculant in a co-dispersion of negatively charged NFC and MTM. The dewatering time was cut from 30 to 2–3 min with incorporation of 10 parts by weight CS, which is interesting from an industrial production perspective.

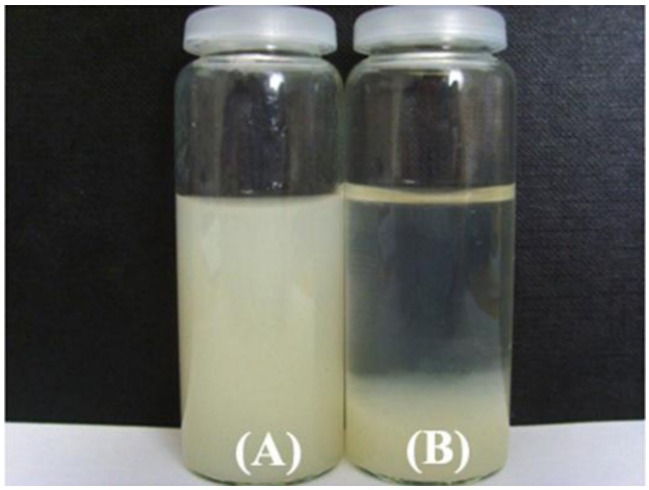

Fig. 1. Photograph of the co-dispersion of MTM50–NFC50 (A) and after dropwise adding of 10 parts by dry weight positively charged chitosan (B) as described in the experimental section.

In order to study the effect of positively charged chitosan on the MTM–NFC nanopaper, chitosan–MTM nanocomposites (CS–MTM) with different CS content were prepared by the same method. XRD spectra of CS–MTM with different CS content are presented in Fig. 2(A). XRD peaks of all silicates shift to lower angle with increased chitosan content. The diffraction peak of MTM (corresponding to d_{001}) moves from 7.0° to 3.8°, corresponding to a d_{001} value of 2.3 nm. The increase of the interlayer distance indicates that positively charged chitosan is intercalated into the gallery interlayers of MTM. This is in contrast to polysaccharides with coiled or helicoidal structures, which are only adsorbed to the external surface of clays (Schultz, van Olphen, & Mumpton, 1985). Furthermore, XRD spectra of NFC–MTM nanopaper with different CS content were obtained, see Fig. 2(A). XRD peaks of all silicates shift to lower angle with increased chitosan content, indicating intercalation as in CS–MTM nanocomposites. The curves of interlayer spacing of MTM with increasing chitosan content for CS–MTM100 and CS–MTM50–NFC50 are presented in Fig. 2(B). At the same weight ratio of chitosan and MTM, the d_{001}value of CS–MTM50–NFC50 decreased slightly comparing with that of CS–MTM. This indicates NFC has no effect on the interaction between chitosan and clay, although NFC may adsorb some positively charged chitosan.

FTIR spectroscopy is used to characterize the interaction between phases. Fig. 3 shows the IR spectra of Na–MTM, chitosan, NFC, nanopaper, CS–MTM (chitosan–clay), CS–NFC (chitosan–cellulose) and CS–MTM50–NFC50 (chitosan–cellulose–clay), in the 4000–1200 cm^{-1} wavenumber range. The pure chitosan shows a very broadband, from 3400 to 3000 cm^{-1} due to well established intermolecular interactions among chitosan units attributed to N–H and O–H stretching. However, for CS20–MTM the peak from 3400 to 3000 cm^{-1} has almost disappeared, which indicates that the intermolecular interaction of chitosan was suppressed by the MTM. It suggests strong interaction between chitosan and MTM and virtually no separate chitosan phase. The frequency of vibrational bands at 1580 cm^{-1} in the chitosan, which corresponds to the deformation vibration (δNH_3) of the protonated amine group, is shifted towards lower frequency values to 1530 cm^{-1} for CS20–MTM. This can be related to the electrostatic interaction between the protonated amine group and negatively charged sites in the clay structure.

For CS20–NFC, the frequency of vibrational bands (δNH3) is shifted to 1530 cm^{-1}, which indicates there is also the electrostatic interaction between protonated amine group and the

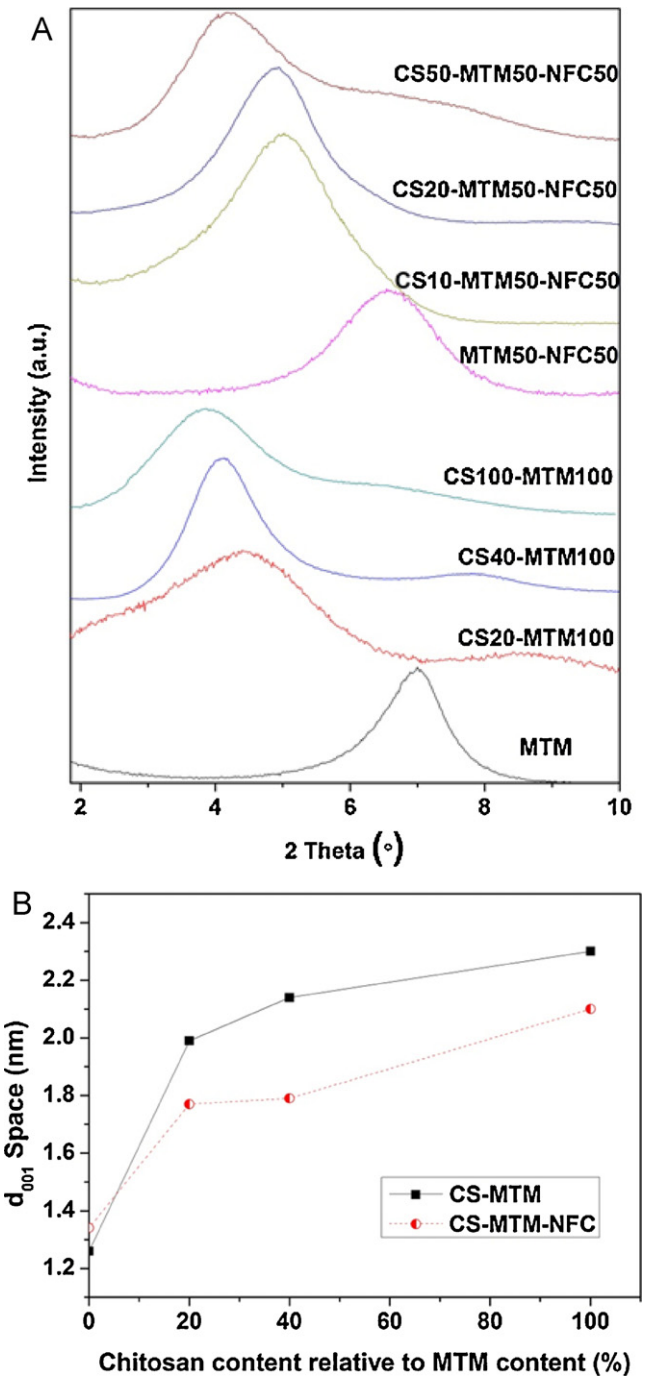

Fig. 2. (A) XRD patterns of CS–MTM chitosan–clay nanocomposites and CS–MTM50–NFC50 clay nanopaper with different contents of chitosan. (B) Interlayer spacing (d_{001}) of MTM with increasing chitosan content for CS–MTM and CS–MTM50–NFC50.

negatively charged sites in the NFC nanofibers. Actually, previous work shows that chitosan is an efficient flocculation agent (Rojas-Reyna et al., 2010) can be adsorbed on the cellulose surface via electrostatic adsorption and non-electrostatic adsorption, such as hydrogen bonding (Dėdinaitė & Ernstsson, 2003; Lundin, Macakova, Dedinaite, & Claesson, 2008; Miklavic & Marcelja, 1988; Schneider et al., 2008; Zhou, Rutland, Teeri, & Brumer, 2007).

Similarly, for CS10–MTM50–NFC50 the frequency of vibrational bands (δNH_3) is shifted to 1530 cm^{-1}. As mentioned above, both MTM and NFC could adsorb chitosan in aqueous solution by electrostatic or hydrogen-bonding interaction. This explains why MTM

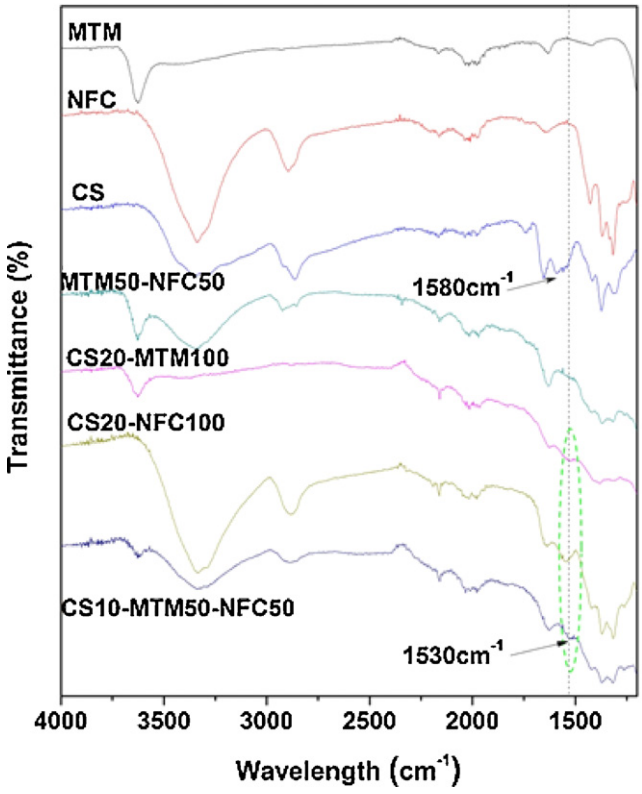

Fig. 3. The FTIR spectra of MTM clay, CS chitosan, NFC, MTM50–NFC50, CS20–MTM100, CS20–NFC100 and CS10–MTM50–NFC50.

and NFC are both flocculated with incorporation of chitosan. It also suggests that MTM and NFC are connected physically via the ionic interaction provided by positively charged chitosan. Chitosan may act as bridging molecules between MTM and NFC. It may in addition bridge individual NFC nanofibers but also act to bridge MTM platelets.

3.2. Morphology of nanocomposites

The film surface morphologies of MTM50–NFC50 and CS10–MTM50–NFC50 were observed by SEM. As shown in Fig. 4(A) and (A′), some large fiber fragments are apparent. The diameter of NFC nanofibers is below 40 nm. A small amount of NFC nanofibers may have re-aggregated during filtration and drying. However, the surface of CS10–MTM50–NFC50 in Fig. 4(B) and (B′) is very homogenous compared with that of MTM50–NFC50. Less aggregation of NFC nanofibers may have occured. The ionic repulsion between MTM and NFC may prevent re-aggregation of NFC during filtration and drying.

Fig. 4(C) and (C′) shows the SEM images of cross-sections of CS10–MTM50–NFC50. Red arrow indicates the thickness direction of film. The horizontal, slightly wavy lines in the micrograph of Fig. 4(C) are characteristic for layered structures (Liu et al., 2011). The layers consist of platelets ordered parallel to the surface. This organization was also observed in bioinspired organic–inorganic composites and has been discussed in detail. (Sellinger et al., 1998; Walther, Bjurhager, Malho, Berglund, et al., 2010; Walther, Bjurhager, Malho, Pere, et al., 2010; Wang, Suo, Evans, Yao, & Aksay, 2001).

3.3. Mechanical properties

Fig. 5(A) and (B) shows the stress–strain curves for nanopapers with increasing chitosan content and nanocomposites with increasing NFC content. Table 2 summarizes the information of weight fractions, porosity, volume fraction and tensile mechanical properties of nanopaper and nanocomposites. As shown in Fig. 5(A), the tensile strength of MTM50–NFC50 is about 124 MPa, and the mechanical behavior shows similarities with that of mineralized tissue in nature, such as nacre (Wang et al., 2001) and bone (Landis, Librizzi, Dunn, & Silver, 1995), as well as artificial materials, such as clay/polyelectrolyte (Tang et al., 2003) and clay/polyvinyl alcohol (Podsiadlo et al., 2007) multilayer nanocomposites prepared by layer-by-layer self-assembly. In Fig. 5(A) the tensile strength increased from 124 MPa (MTM50–NFC50) to 134 MPa (CS10–MTM50–NFC50) with incorporation of 10 parts by weight of chitosan. The load transfer between MTM and NFC is probably improved due to the ionic interaction provided by cationic chitosan binder. Increasing the chitosan content further leads to decreased tensile strength of nanopaper due to the soft characteristics of chitosan polymer itself, see Fig. 5(A). It is interesting to note that the present strength and strain to failure, see Table 2, are much higher than for recently reported vacuum-filtrated chitosan–clay nanocomposites with 65 wt% clay content (132 MPa compared with 76 MPa, and 2.2% compared with 0.97%) (Yao et al., 2010).

The effect of NFC content on the mechanical properties of CS–MTM nanocomposites was also studied. The amount of CS and MTM was fixed at 50 parts by weight for each. The NFC content was 0, 4, 8 and 12 parts by weight, see Table 1. Fig. 5(B) presents changes in tensile modulus and strength with NFC content. Compared with CS50–MTM50, the tensile modulus of CS50–MTM50–NFC12 increased from 5.9 GPa to 9.7 GPa and the tensile strength increased from 55 MPa to 127 MPa. Note also the dramatic effect of adding only 4 parts by weight of NFC. NFC has a strong reinforcement effect on CS–MTM nanocomposites. One reason may be that a significant fraction of CS is intercalated into the MTM galleries, whereas NFC serves to link MTM platelets and improve stress transfer, probably aided by CS in matrix function. Although there is significant complexity in a nanocomposite with three components, the combination of CS, NFC and MTM undoubtedly results in highly favorable mechanical properties. A higher CS content increases strain to failure, although the strength decreases, see Fig. 5(A).

3.4. Thermal properties of nanocomposites

TGA curves of MTM, NFC, CS, and the nanocomposites are presented in Fig. 6. For MTM50–NFC50, degradation rate is decreased

Table 2
Weight fractions, porosity, volume fraction and mechanical properties of nanocomposites.

Sample codes	W_f of CS/MTM/NFC (%)	Porosity (%)	V_f of CS/MTM/NFC (%)	Tensile strength (MPa)	Tensile modulus (GPa)	Elongation at break (%)
MTM50–NFC50	0/50/50	24	0/26/50	123 ± 4	7.5 ± 0.2	2.8 ± 0.2
CS10–MTM50–NFC50	9.0/45.5/45.5	20	10/24/46	132 ± 2	7.8 ± 0.1	2.2 ± 0.2
CS20–MTM50–NFC50	16.6/41.7/41.7	19	19/21/41	102 ± 4	6.4 ± 0.1	3.2 ± 0.1
CS50–MTM50–NFC50	33.3/33.3/33.3	18	35/16/31	72 ± 7	4.2 ± 0.4	4.5 ± 0.6
CS50–MTM50	50/50/0	10	62/28/0	56 ± 3	5.9 ± 0.3	1.2 ± 0.1
CS50–MTM50–NFC4	48.4/48.1/3.8	10	59/27/4	103 ± 2	8.5 ± 0.1	2.4 ± 0.2
CS50–MTM50–NFC8	46.3/46.3/7.4	11	56/25/8	110 ± 7	9.0 ± 0.2	1.6 ± 0.2
CS50–MTM50–NFC12	44.6/44.6/10.8	12	53/24/11	128 ± 7	9.7 ± 0.1	1.8 ± 0.2

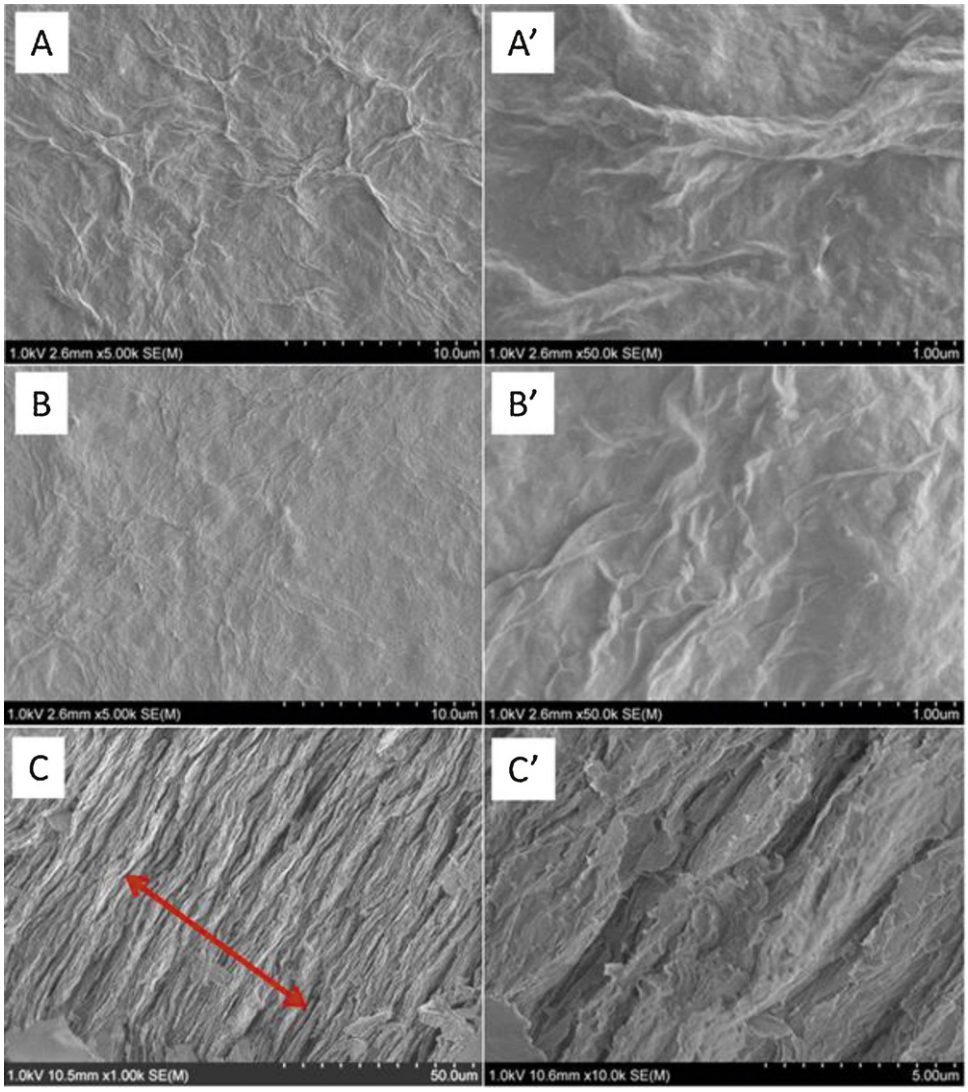

Fig. 4. SEM micrographs of the surface morphology of MTM50–NFC50 (A and A′) and CS10–MTM50–NFC50 (B and B′). Note differences in scale; 10 μm scale bar (A and B), 1 μm scale bar (A′ and B′); and SEM images of the cross section of a fracture surface of CS10–MTM50–NFC50 (C and C′) (arrow indicates the thickness direction of nanopaper).

compared with pure NFC. Clay platelets predominantly ordered parallel to the surface hinder oxygen diffusion and also mass transport of decomposition products. However, T_{onset} (the temperature at onset of decomposition when the weight loss is 10% of total weight) of CS10–MTM50–NFC50 and CS20–MTM50–NFC50 decreased about 50 °C compared with that of MTM50–NFC50, see Table 3, due to degradation of chitosan. From Table 3, T_{onset} of CS is 239 °C. Clay platelets limit the decomposition of CS as is apparent in the CS40–MTM curve.

3.5. Oxygen gas-barrier properties of nanocomposites

Oxygen gas-barrier properties of NFC, MTM50–NFC50 and CS10–MTM50–NFC50 were measured at 0%, 50% and 95% relative humidity (RH), see Table 4. For all, the oxygen transmission rate (OTR) at 0% RH is below the detection limit, which is around 0.001 $cm^3\ mm\ m^{-2}\ day^{-1}\ atm^{-1}$. This indicates better performance than other biodegradable polymers or synthetic polyvinyl alcohol. The combination of ordered cellulose regions in NFC and high MTM volume fraction organized in a nacre-like layered structure provide this effect. The OTR of NFC and MTM50–NFC50 at 50% RH was 0.048 and 0.046 $cm^3\ mm\ m^{-2}\ day^{-1}\ atm^{-1}$, respectively. Both NFC and intercalated MTM structures are swollen by water adsorp-

Table 4
Oxygen transmission rate (OTR, $cm^3\ mm\ m^{-2}\ day^{-1}\ atm^{-1}$) of NFC, MTM50–NFC50 and CS10–MTM50–NFC50 under 0%, 50% and 95% relative humidity (RH) and 100% oxygen conditions.

Samples	OTR at 0% RH	OTR at 50% RH	OTR at 95% RH
NFC	N/A	0.048	17.8
MTM50–NFC50	N/A	0.046	3.5
CS10–MTM50–NFC50	N/A	0.025	2.5

N/A, OTR at 0% RH 100% O_2 for these materials was below detection limit (0.001 $cm^3\ mm\ m^{-2}\ day^{-1}\ atm^{-1}$).

Table 3
Temperature at onset of decomposition (10% weight loss) in O_2 flow.

	CS	NFC	CS40–MTM100	MTM50–NFC50	CS10–MTM50–NFC50	CS20–MTM50–NFC50
Onset of degradation (10% weight loss)	239 °C	302 °C	251 °C	311 °C	258 °C	253 °C

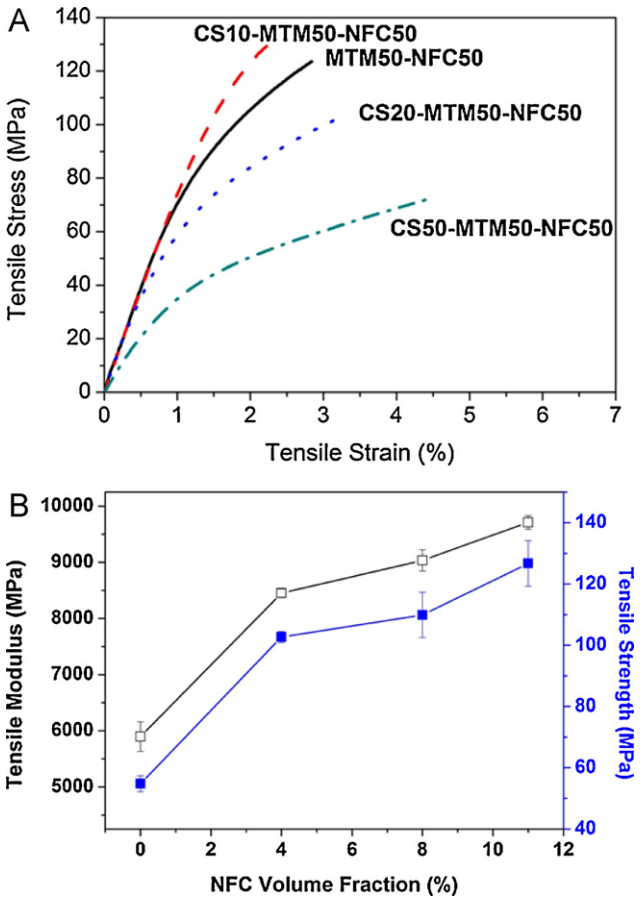

Fig. 5. Mechanical properties. (A) The stress–strain curves for CS–MTM50–NFC50 with different contents of chitosan. (B) Tensile modulus and strength of CS50–MTM50 as a function of NFC volume fraction. The porosity is 10–12%, see Table 2.

tion. When 10% chitosan was added, the OTR of MTM50–NFC50 decreased slightly. When the RH was increased to 95%, the OTR of NFC increased dramatically, about 370 times compared with the value at 50% RH. Water molecules above a certain water activity level can disrupt hydrogen bonding and van der Waals interactions, and create space for permeation of oxygen and an increased diffusion rate of oxygen. The OTR of MTM50–NFC50 is lower than that of NFC, as expected from the increased diffusion

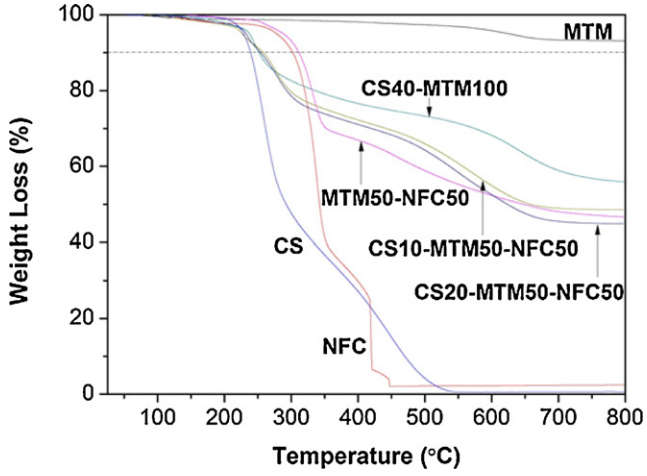

Fig. 6. TGA curves of MTM, NFC, CS, and the different nanocomposites presented in Table 1.

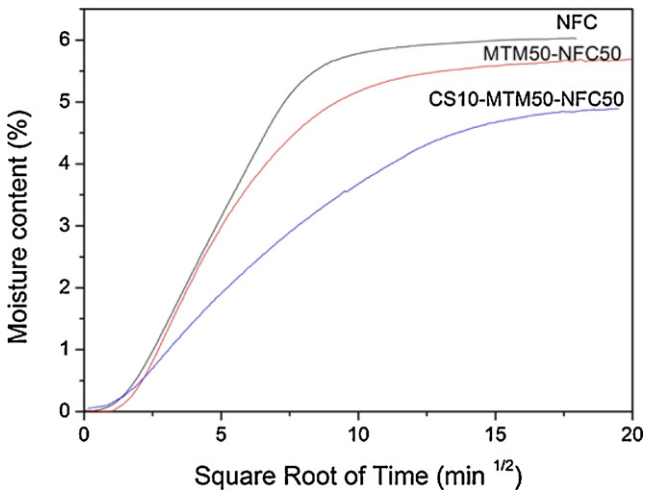

Fig. 7. DVS moisture content vs. square root of time curves of NFC, MTM50–NFC50 and CS10–MTM50–NFC50 at 50% relative humidity and 30 °C.

length along the tortuous diffusion path in a nacre-like structure. The OTR of CS10–MTM50–NFC50 is decreased further compared with MTM50–NFC50 as 10% chitosan is added. CS possibly restricts swelling in the system by linking the constituents.

3.6. Kinetics of water sorption

The kinetics of water sorption of NFC, MTM50–NFC50 and CS10–MTM50–NFC50 were measured. Fig. 7 presents moisture content vs. square root of time at 50% relative humidity and 30 °C. The rate of moisture uptake is somewhat lower for MTM50–NFC50 compared with NFC. It is interesting to note that the addition of 10 wt% CS (CS10–MTM50–NFC50) decreased moisture uptake rate substantially compared with NFC or MTM50–NFC50. Most likely swelling is reduced, due to lower hydrophilicity of CS or a reduction in the number of accessible hydroxyl groups since CS interacts with NFC and MTM.

4. Conclusions

This study continues the exploration of clay nanopaper biocomposites with nacre-like structure prepared by a papermaking approach. The addition of 10 parts by weight of chitosan to a hydrocolloidal MTM50–NFC50 clay–nanofiber dispersion leads to immediate flocculation due to the ionic interaction between the constituents. The filtration time during processing was therefore dramatically reduced. The three-phase CS–MTM–NFC clay nanopaper indeed formed a multilayered nacre-like structure. The tensile strength increased slightly with the addition of 10 wt% chitosan. MTM platelets strongly improved the thermostability of the materials and OTR is very low in dry conditions. Chitosan probably decreases moisture swelling in clay nanopaper, since CS addition decreases OTR at 95% relative humidity. In chitosan–clay nanocomposites, addition of small amounts of NFC dramatically improves strength and modulus. This is most likely because NFC improves stress transfer between the inorganic platelets and the organic chitosan–NFC “matrix”. Chitosan-modified clay nanopaper has potential applications in packaging, as films or coatings and as molded laminates. Most likely, there is considerable potential to improve the already impressive properties of chitosan–clay–NFC nanopaper structures through improved stress transfer by stronger molecular clay platelet interactions with the surrounding chitosan–NFC matrix.

Acknowledgement

The BiMaC Innovation center is gratefully acknowledged for financial support of Dr. Andong Liu.

References

Bonderer, L. J., Studart, A. R., & Gauckler, L. J. (2008). Bioinspired design and assembly of platelet reinforced polymer films. *Science*, *319*(5866), 1069–1073.

Darder, M., Colilla, M., & Ruiz-Hitzky, E. (2003). Biopolymer–clay nanocomposites based on chitosan intercalated in montmorillonite. *Chemistry of Materials*, *15*(20), 3774–3780.

Dėdinaitė, A., & Ernstsson, M. (2003). Chitosan–SDS interactions at a solid–liquid interface: Effects of surfactant concentration and ionic strength. *The Journal of Physical Chemistry B*, *107*(32), 8181–8188.

Divakaran, R., & Pillai, V. N. S. (2001). Flocculation of kaolinite suspensions in water by chitosan. *Water Research*, *35*(16), 3904–3908.

Fernandes, S. C. M., Freire, C. S. R., Silvestre, A. J. D., Gandinia, C. P. A. N., Berglund, L. A., & Salmén, L. (2010). Transparent chitosan films reinforced with a high content of nanofibrillated cellulose. *Carbohydrate Polymers*, *81*(2), 394–401.

Günister, E., Pestreli, D., Ünlü, C. H., Atıcı, O., & Güngör, N. (2007). Synthesis and characterization of chitosan–MMT biocomposite systems. *Carbohydrate Polymers*, *67*(3), 358–365.

Henriksson, M., Henriksson, G., Berglund, L. A., & Lindström, T. (2007). An environmentally friendly method for enzyme-assisted preparation of microfibrillated cellulose nanofibers. *European Polymer Journal*, *43*(8), 3434–3441.

Huang, X. S., & Netravali, A. (2007). Characterization of flax fiber reinforced soy protein resin based green composites modified with nano-clay particles. *Composites Science and Technology*, *67*(10), 2005–2014.

Landis, W. J., Librizzi, J. J., Dunn, M. G., & Silver, F. H. (1995). A study of the relationship between mineral content and mechanical properties of Turkey gastrocnemius tendon. *Journal of Bone and Mineral Research*, *10*(6), 859–867.

Liu, A. D., Walther, A., Ikkala, O., Belova, L., & Berglund, L. A. (2011). Clay nanopaper with tough cellulose nanofiber matrix for fire-retardancy and gas barrier functions. *Biomacromolecules*, *12*(3), 633–641.

Lundin, M., Macakova, L., Dedinaite, A., & Claesson, P. (2008). Interactions between chitosan and SDS at a low-charged silica substrate compared to interactions in the bulk: The effect of ionic strength. *Langmuir*, *24*(8), 3814–3827.

Maiti, P., Yamada, K., Okamoto, M., Ueda, K., & Okamoto, K. (2002). New polylactide/layered silicate nanocomposites: Role of organoclays. *Chemistry of Materials*, *14*(11), 4654–4661.

Miklavic, S. J., & Marcelja, S. (1988). Interaction of surfaces carrying grafted polyelectrolytes. *The Journal of Physical Chemistry*, *92*(23), 6718–6722.

Papineau, A. M., Hoover, D. G., Knorr, D., & Farkas, D. F. (1991). Antimicrobial effect of water-soluble chitosans with high hydrostatic pressure. *Food Biotechnology*, *5*(1), 45–57.

Park, H. M., Liang, X. M., Mohanty, A., Misra, M., & Drzal, T. L. (2004). Effect of compatibilizer on nanostructure of the biodegradable cellulose acetate/organoclay nanocomposites. *Macromolecules*, *37*(24), 9076–9082.

Podsiadlo, P., Kaushik, A. K., Arruda, E. M., Waas, A. M., Shim, B. S., Xu, J., et al. (2007). Ultrastrong and stiff layered polymer nanocomposites. *Science*, *318*(5847), 80–83.

Pranger, L., & Tannenbaum, R. (2008). Biobased nanocomposites prepared by in situ polymerization of furfuryl alcohol with cellulose whiskers or montmorillonite clay. *Macromolecules*, *41*(22), 8682–8687.

Ray, S. S., Maiti, P., Okamoto, M., Yamada, K., & Ueda, K. (2002). New polylactide/layered silicate nanocomposites. 1. Preparation, characterization, and properties. *Macromolecules*, *35*(8), 3104–3110.

Ray, S. S., Okamoto, K., & Okamoto, M. (2003). Structure–property relationship in biodegradable poly(butylenes succinate)/layered silicate nanocomposites. *Macromolecules*, *36*(7), 2355–2367.

Rojas-Reyna, R., Schwarz, S., Heinrich, G., Petzold, G., Schütze, S., & Jörg, B. (2010). Flocculation efficiency of modified water soluble chitosan versus commonly used commercial polyelectrolytes. *Carbohydrate Polymers*, *81*, 317–322.

Roussya, J., Voorenb, M. V., Dempseyc, B. A., & Guibal, E. (2005). Influence of chitosan characteristics on the coagulation and the flocculation of bentonite suspensions. *Water Research*, *39*(14), 3247–3258.

Schneider, C., Jusufi, A., Farina, R., Li, F., Pincus, P., Tirrell, M., et al. (2008). Microsurface potential measurements: Repulsive forces between polyelectrolyte brushes in the presence of multivalent counterions. *Langmuir*, *24*(19), 10612–10615.

Schultz, L. G., van Olphen, H., & Mumpton, F. A. (1985). *The clay minerals society*. Bloomington: IN., pp. 375–381.

Sehaqui, H., Liu, A. D., Zhou, Q., & Berglund, L. A. (2010). Fast preparation procedure for large, flat cellulose and cellulose/inorganic nanopaper structures. *Biomacromolecules*, *11*(9), 2195–2198.

Sellinger, A., Weiss, P. M., Nguyen, A., Lu, Y. F., Assink, R. A., Gong, W. L., et al. (1998). Continuous self-assembly of organic–inorganic nanocomposite coatings that mimic nacre. *Nature*, *394*, 256–260.

Tang, Z., Kotov, N. A., Magonov, S., & Ozturk, B. (2003). Nanostructured artificial nacre. *Nature Materials*, *2*, 413–418.

Walther, A., Bjurhager, I., Malho, J. M., Berglund, L. A., & Ikkala, O. (2010). Supramolekulare Kontrolle der mechanischen Eigenschaften feuerabschirmender biomimetischer Perlmuttanaloga. *Angewandte Chemie International Edition*, *122*, 6593–6599.

Walther, A., Bjurhager, I., Malho, J. M., Pere, J., Berglund, L. A., & Ikkala, O. (2010). Large-area, lightweight and thick biomimetic composites with superior material properties via fast, economic, and green pathways. *Nano Letters*, *10*(8), 2742–2748.

Wang, R. Z., Suo, Z., Evans, A. G., Yao, N., & Aksay, I. A. (2001). Deformation mechanism in nacre. *Journal of Materials Research*, *16*, 2485–2493.

Wang, X. Y., Du, Y. M., Yang, J. H., Wang, X. H., Shi, X. W., & Hu, Y. (2006). Preparation, characterization and antimicrobial activity of chitosan/layered silicate nanocomposites. *Polymer*, *34*(19), 6738–6744.

Yao, H. B., Tan, Z. H., Fang, H. Y., & Yu, S. H. (2010). Artificial nacre-like bionanocomposite films from the self-assembly of chitosan–montmorillonite hybrid building blocks. *Angewandte Chemie International Edition*, *49*(52), 1–6.

Zhou, Q., Rutland, M. W., Teeri, T. T., & Brumer, H. (2007). Xyloglucan in cellulose modification. *Cellulose*, *14*(6), 625–641.